

A.R. Atmeh<sup>1</sup>, E.Z. Chong<sup>1</sup>, G. Richard<sup>2</sup>,  
F. Festy<sup>1</sup>, and T.F. Watson<sup>1\*</sup>

<sup>1</sup>Biomaterials, Biomimetics and Biophotonics, King's College London Dental Institute, Floor 17 Tower Wing, Guy's Hospital, London Bridge, London SE1 9RT, UK; and <sup>2</sup>Septodont, Saint Maur des Fossés Cedex, France; \*corresponding author, timothy.f.watson@kcl.ac.uk

*J Dent Res* 91(5):454-459, 2012

## ABSTRACT

The interfacial properties of a new calcium-silicate-based coronal restorative material (Biodentine™) and a glass-ionomer cement (GIC) with dentin have been studied by confocal laser scanning microscopy (CLSM), scanning electron microscopy (SEM), micro-Raman spectroscopy, and two-photon auto-fluorescence and second-harmonic-generation (SHG) imaging. Results indicate the formation of tag-like structures alongside an interfacial layer called the “mineral infiltration zone”, where the alkaline caustic effect of the calcium silicate cement's hydration products degrades the collagenous component of the interfacial dentin. This degradation leads to the formation of a porous structure which facilitates the permeation of high concentrations of Ca<sup>2+</sup>, OH<sup>-</sup>, and CO<sub>3</sub><sup>2-</sup> ions, leading to increased mineralization in this region. Comparison of the dentin-restorative interfaces shows that there is a dentin-mineral infiltration with the Biodentine, whereas polyacrylic and tartaric acids and their salts characterize the penetration of the GIC. A new type of interfacial interaction, “the mineral infiltration zone”, is suggested for these calcium-silicate-based cements.

**KEY WORDS:** Biodentine, glass-ionomer cement, interfaces, Raman, confocal microscopy, second harmonic generation.

DOI: 10.1177/0022034512443068

Received December 12, 2011; Last revision February 23, 2012; Accepted February 25, 2012

© International & American Associations for Dental Research

# Dentin-cement Interfacial Interaction: Calcium Silicates and Polyalkenoates

## INTRODUCTION

Torabinejad first developed mineral trioxide aggregate (MTA) as a surgical root repair material in 1993 (Lee *et al.*, 1993). Subsequently, significant interest has been shown in MTA, due to its biocompatibility (Camilleri *et al.*, 2004) and potential bioactivity (Tay *et al.*, 2007). More recently, a new calcium-silicate restorative material called Biodentine™ has been produced by Septodont (Saint Maur des Fosses, France), to be used not only as an endodontic repair material but also as a coronal restorative material for dentin replacement.

Biodentine (henceforth used in the text for brevity) is composed of a highly purified tricalcium silicate powder that contains small proportions of dicalcium silicate, calcium carbonate, and a radiopaquer. It is dispensed in a fixed powder:liquid proportion, providing a shorter setting time of 12 min (manufacturer's data sheets), compared with the 3 to 4 hrs of MTA (Torabinejad *et al.*, 1995). Because of components similar to those of Portland Cement, it may be assumed that Biodentine sets through a hydration reaction that involves dissolution of calcium silicate granules to produce calcium hydroxide and calcium silicate hydrates, which form the matrix that holds unhydrated granules and contains water-filled micro-spaces where the calcium hydroxide distributes, which provides the high alkalinity (Taylor, 1997; Tsvilis *et al.*, 2002; Kjellsen and Justnes, 2004; Camilleri *et al.*, 2011). However, the setting reactions involved in the complex mixture of Biodentine have not been fully investigated.

Glass-ionomer cements (GIC) are also water-based restorative materials. GIC setting, however, is an acid-base reaction that involves the formation of polyalkenoate salts as a result of the acid attack on fluoroaluminosilicate glass fillers. Being of an acidic nature, GICs are considered self-etching cements, and on wet dentin, trigger an ionic exchange with the interface, accompanied by water movement between the two substrates (Watson, 1999).

The null hypothesis is that the water-based cements in this study have identical cement and mineral diffusion into the dentin.

## MATERIALS & METHODS

For the evaluation of the interface between human dentin and Biodentine/GIC, we used confocal reflection and fluorescence microscopy to observe interface microporosity (Watson *et al.*, 2008), two-photon auto-fluorescence and second-harmonic-generation (SHG) imaging to detect collagen denaturation (Chen *et al.*, 2007), SEM for microstructural characterization, and micro-Raman spectroscopy for chemical mapping of the interfaces (Martinez-Ramirez *et al.*, 2006; Ibáñez *et al.*, 2007).

## Sample Preparation

Occlusal cavities were prepared in 49 teeth extracted after the appropriate informed consent was obtained from the patients (East Central London Research Ethics Committee 1, 10/H0721/55). Cavities were prepared by the use of a high-speed handpiece with a type 012 diamond bur, and standardized to  $7 \times 4 \times 4$  mm, and a cavosurface angle of  $90^\circ$ . All teeth were then cleaned for 5 min in an ultrasonic bath. Thirty-one cavities were filled with the Biodentine, mixed as *per* manufacturer's instructions for 30 sec with an amalgamator. In 18 teeth, cavities were filled with a conventional GIC-Fuji IX (GC Corporation, Tokyo, Japan) without the application of dentin conditioner, and cements were applied to the cavities directly after mixing and cavity preparation by means of a plastic instrument and adapted in an amalgam condenser. All samples were kept wet inside an incubator at  $37^\circ\text{C}$  for 24 hrs before being labeled and imaged. In each tooth, the root was cut just below the cementum-enamel junction by means of a water-cooled diamond wafering blade (Benetec Limited, London, UK). Additionally, 10 dentin discs of 1 mm thickness were cut from five extracted human teeth; mixed Biodentine was applied on five discs and GIC on the others. The discs were kept for 4 days in distilled water at  $37^\circ\text{C}$  before they were fractured perpendicular to the interface and gold-sputter-coated. The fractured surfaces were imaged by scanning electron microscopy (Hitachi S3500N, Hitachi High Technologies, Maidenhead, UK).

## Imaging

Samples were divided into four groups:

**Micro-permeability group** ( $n = 15$ ): An aqueous 0.25% solution of Rhodamine-B (R6626-Sigma-Aldrich, Dorset, UK) was put in the open pulp chambers of the Biodentine ( $n = 10$ ) and GIC ( $n = 5$ ) samples and placed upside-down in a damp environment. The dye was left for 3 hrs to permeate toward the interface.

**Double-labeling group** ( $n = 15$ ): Biodentine ( $n = 10$ ) and GIC ( $n = 5$ ) cements were mixed with 1 mg of a fluorescein dye powder (F6377 Sigma-Aldrich, Dorset, UK) and applied to cavities one day before the micro-permeability test was conducted.

After being stained, all samples were rinsed with distilled water, sectioned vertically, then ground with carborundum paper up to 1200 grit.

A confocal tandem scanning microscope (TSM) (Noran Instruments, Middleton, WI, USA) was used to image the samples of the first group, with a  $\times 60/1.4$  numerical aperture (NA) and  $\times 100/1.4$  NA oil immersion (OI) objective lens with a 546-nm band-pass excitation and a 600-nm long-pass emission filters. Confocal widefield images were recorded with an electron multiplying iXon 885 EM-CCD (Andor Technology, Northern Ireland, UK). Samples of the second group were imaged by confocal laser scanning microscopy (CLSM) Leica TCS SP2 (Leica Microsystems, Heidelberg GmbH, Germany) with an  $\times 100/1.4$  NA OI objective lens in conjunction with 488-nm laser excitation and 530-nm emission filters for the fluorescein dye, and 568-nm laser excitation and 640-nm emission filters for the Rhodamine-B.

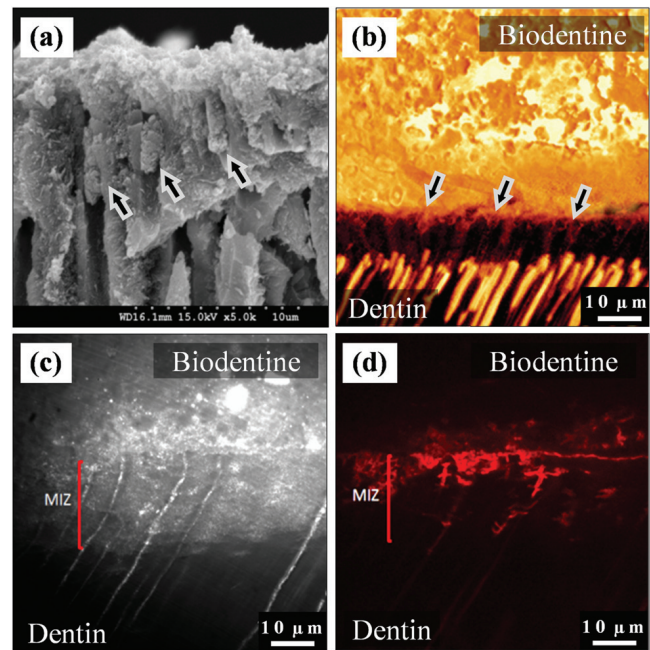


**Figure 1.** Interfacial characteristics. (a) SEM micrograph of fractured dentin beneath a Biodentine restoration. Tag-like structures were detected forming within the dentinal tubules (arrows). (b) Fluorescence-mode CLSM image showing the cement tags, which appear on the interfacial surface of the fluorescein-labeled Biodentine (above) after it was pulled away from dentin due to desiccation.  $63\times/1.4$  NA OI. (c) Reflection-mode TSM image for the dentin/Biodentine interface. The mineral infiltration zone (MIZ) appears as a band of highly reflective dentin beneath the interface, indicating a change in dentin's mineral content within this zone. The fluorescence-mode image of the same area (d) shows the distribution of Rhodamine-B dye, which permeated from the pulp chamber into the interface and cement.

From four randomly selected samples of each material, four interfacial images were made *per* sample. Each image was adjusted so that the interface was exactly horizontal, and the average vertical intensity profile was calculated to allow unbiased fluorescence infiltration measurements to be made.

**Stain-free group** ( $n = 10$ ): Biodentine ( $n = 5$ ) and GIC ( $n = 5$ ) filled teeth were sectioned and prepared for imaging as described above. Using an in-house multi-photon microscope, we performed stain-free imaging for both tissue auto-fluorescence (830-nm excitation and 500-nm emission) and collagen second-harmonic generation (950-nm excitation, 475-nm emission).

**Micro-Raman Spectroscopy group** ( $n = 9$ ): Nine samples (6 Biodentine and 3 GIC) were kept in distilled water at  $37^\circ\text{C}$  for 8 days. A flat sectioned surface was created by means of a diamond wafering blade to expose the interface between the dentin and the cement, ground as described above and measured 1 and 8 days following cement placement.

For each sample, a Raman map of the material/dentin interface, with a resolution of  $0.9 \mu\text{m}$  across the interface, was recorded with the fast StreamLine™ mapping provided with the inVia micro-Raman spectrometer (Renishaw plc, Wotton-under-Edge, UK). A water immersion  $\times 60/1.2$  NA objective lens Plan Apo VC was used with a 785-nm laser source (25 mW line

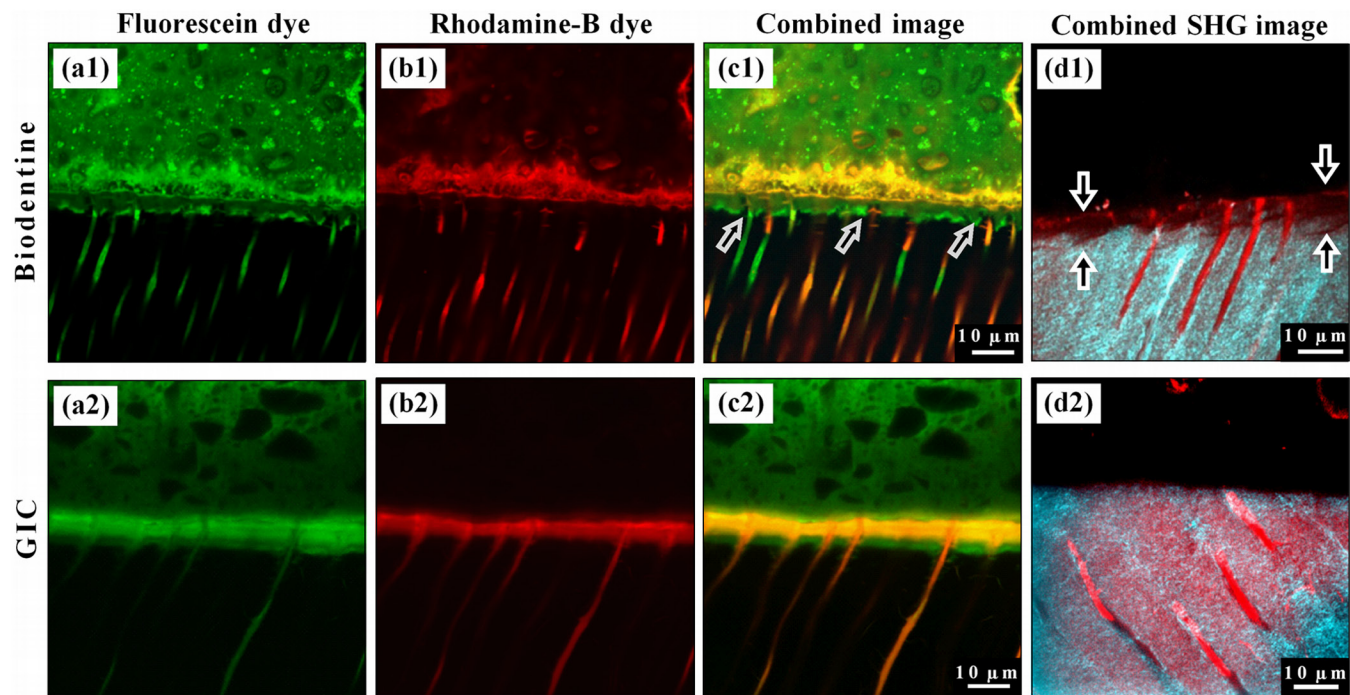


**Figure 2.** Representative fluorescence-mode CLSM images for the interfaces of Biodentine and GIC cements (upper side of each image) with the dentin (lower side). **(a1)** Distribution of the fluorescein dye labeling the Biodentine cement shows a band of richly dye-infiltrated dentin just beneath the interface. This band cannot be seen with Rhodamine-B micro-permeability **(b1)**, where the dye permeated through this band and diffused into the cement above the interface without any mixing with the fluorescein. This band is believed to be formed as a result of the strong alkaline effect of calcium hydroxide leaching out of the cement, and it corresponds to the MIZ. **(c1)** Dye-deficient areas can be seen within this zone (arrows), which represent the un-affected peritubular dentin. **(a2)** Fluorescein distribution in GIC samples also shows a richly dye-infiltrated dentin band, but this band was formed due to the acidic effect of GIC, which affected both intertubular and peritubular dentin. **(b2)** Rhodamine-B permeating from the pulp has also infiltrated this band, which diffused laterally through the affected tubular walls and mixed with the fluorescein as shown in **(c2)**. **(d1)** Second-harmonic-generation (SHG) signal, originating from the intertubular collagen (cyan), is weak and almost absent in the interfacial dentin beneath the Biodentine (arrows) when superimposed over the dentin's autofluorescence signal (red), which reflects its actual margin. Notice the preserved tubular structure of dentin in this zone, unlike the images for GIC samples **(d2)**, where the SHG signal has the same distribution as the dentin's autofluorescence signal.

illumination) and a 600 lines/mm diffraction grating. All Raman maps were uploaded into in-house curve-fitting software to fit the cements' characteristic peaks, generate intensity line profiles in the crown-pulp direction, and calculate the diffusion lengths.

## RESULTS

### Tag-like Structures

Representative SEM (Fig. 1a) and confocal (Fig. 1b) images of Biodentine samples showed tag-like structures within the dentinal tubules just beneath the interface. Fig. 1b shows these tags on the bottom surface of a detached Biodentine filling. There was little evidence of tag-like structures beneath the GIC restorations.

### Interfacial Interactions

A representative reflection-mode TSM confocal image for the dentin/Biodentine interface (Fig. 1c) shows a bright band, ranging between 5 and 15  $\mu\text{m}$ , noticed within the structure of dentin directly below and along the interface, which indicates a change

in the reflective properties of dentin at this area. A fluorescence image of the same area (Fig. 1d) shows the permeability of the dye solution.

Representative CLSM fluorescence images for the double-labeled Biodentine samples show a richly dye-infiltrated layer ( $6.5 \mu\text{m} \pm 0.6 \mu\text{m}$  wide) positioned just beneath the interface (Fig. 2a1). Fig. 2b1 shows the distribution of Rhodamine-B permeating from the pulp and diffusing into the cement, but barely into the intertubular dentin. Fig. 2c1 is a combined image. Similarly, the GIC samples exhibited a richly dye-infiltrated layer ( $14.5 \mu\text{m} \pm 1.9 \mu\text{m}$  wide) visible within the structure of dentin in both the fluorescent images (Figs. 2a2, 2b2), which show similar dye distribution when combined (Fig. 2c2). The combined two-photon auto-fluorescence and SHG images of the Biodentine samples showed a band of low SHG signal intensity due to the alteration of the collagen fibers close to the interface by this material (Fig. 2d1), not seen in the GIC samples (Fig. 2d2).

In the SEM images, a band of structurally altered dentin was visible just below the interface in the Biodentine samples (Fig. 3a), but not in the GIC samples (Fig. 3b). Within this 10- to 20- $\mu\text{m}$ -wide band, microstructural alterations were noticeable but were absent on the opposite surfaces of the discs, where no



cement was applied (Figs. 3c, 3d). In the surfaces exposed to Biodentine, the dentinal tubules appear blocked and did not open to the surface, unlike the tubules in the clean, unexposed surfaces.

### Chemical Mapping

The  $1082\text{-cm}^{-1}$  carbonate Raman peak (Fig. 4), representing the stretching mode of the C-O bond in the carbonate group (Martinez-Ramirez *et al.*, 2006), was associated with the presence of calcium carbonate, originating either from calcium hydroxide carbonation or present originally in the Biodentine. The GIC's broad peak (Fig. 4), located at  $1262\text{ cm}^{-1}$ , corresponds to the overlapping of smaller peaks that represent the polyacrylic (PAA) and tartaric acids and their salts (Young *et al.*, 2000). The intensity of both cements' peaks declined at points located beneath the interface, but in different patterns. This decline was gradual throughout the whole depth for the GIC samples but was followed by a sudden drop in the Biodentine samples. The penetration depths of Biodentine and GIC measured  $48 \pm 10\ \mu\text{m}$  and  $51 \pm 6\ \mu\text{m}$ , respectively.

### DISCUSSION

In the dentin/Biodentine interface, tag-like microstructures were detectable in the fractured samples in both confocal (Fig. 1b) and SEM images (Fig. 1a). These tags have previously been reported in MTA (Reyes-Carmona *et al.*, 2009) and Biodentine (Han and Okiji, 2011). Following hydration, the flowable consistency of the cement aids its penetration through opened dentinal tubules to crystallize over time within their structure (Weller *et al.*, 2008), participating in the mechanical properties of the interface (Reyes-Carmona *et al.*, 2010).

However, the confocal images of the Biodentine samples also showed an interfacial layer within the structure of dentin, just beneath the cement. This layer appears both as a highly reflective band (Fig. 1c) and a richly dye-infiltrated band flooded by fluorophores leaching from the cement (Figs. 2a1, 2c1). This layer, which we call the "mineral infiltration zone" (MIZ), may be associated with an altered intertubular microstructure leading to a change in the optical properties of the interfacial dentin. This layer is confirmed by the SEM micrographs that showed the same band of structurally altered dentin immediately beneath the Biodentine (Fig. 3a). The GIC samples (Fig. 3b) and the dentin of the opposite surfaces of the discs (Figs. 3c, 3d), however, did not show such changes.

The MIZ conceptually resembles the inter-diffusion zone in the interface between dentin and adhesives (Ferrari and

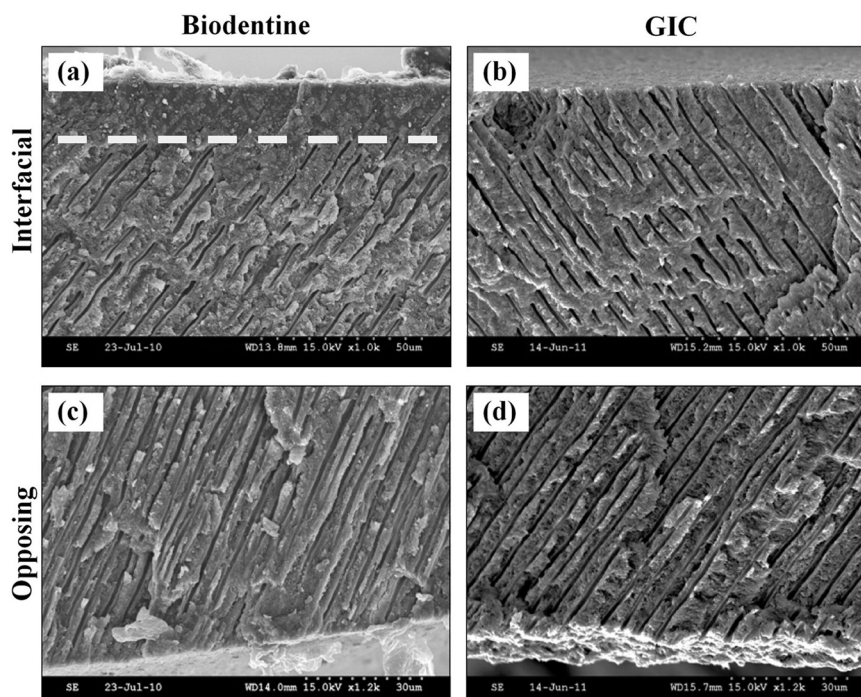


**Figure 3.** SEM micrographs of the fractured dentin discs which were exposed to Biodentine (a) or GIC (b). A band of structurally altered dentin extends along the interface, as can be seen by the obliterated dentin tubules above the dotted line in (a), when compared with dentin of the opposite surface of the disc, where no cement was applied (c). (b) No structural changes can be detected in the dentin beneath GIC when compared with dentin of the opposite surface (d).

Davidson, 1996), or the ion exchange layer that appears interfacially between dentin and GIC (Wilson *et al.*, 1983) (Fig. 2c2). However, the mechanism for the formation of the MIZ might be different, given the alkaline nature of unset calcium-silicate cements compared with acidic GICs. The MIZ could be attributed to a dual effect of the calcium-hydroxide-releasing cement: first, an alkaline caustic etching, followed by mineral diffusion.

Calcium hydroxide is a highly alkaline material ( $\text{pH} = 13$ ) and could induce a caustic degradation effect on exposed collagen. This effect is mediated by the breakdown of intermolecular bonds in the collagen fibrils, increasing their water absorption and leading to swelling (Bowes, 1950; Kemp and Tristram, 1971). Andersen *et al.* (1992) referred to the same effect in explaining the decrease in the weight of pulpal tissues when exposed to calcium hydroxide. They attributed this change to the breakdown of ionic bonds in proteins and destruction of their tertiary structures. The denaturing effect of calcium hydroxide was also suggested by Andreasen *et al.* (2002) and White *et al.* (2002), who noticed a negative effect of this paste on root mechanical properties. This was confirmed by the reduced, or even absent, second-harmonic-generation signal originating from dentin within the MIZ (Fig. 2d1), indicating changes in the collagen conformation (Sun *et al.*, 2006), unlike in GIC samples (Fig. 2d2), where the SHG signal was not affected.

The high alkalinity of hydrated Biodentine could therefore induce a caustic denaturing and permeability of the organic

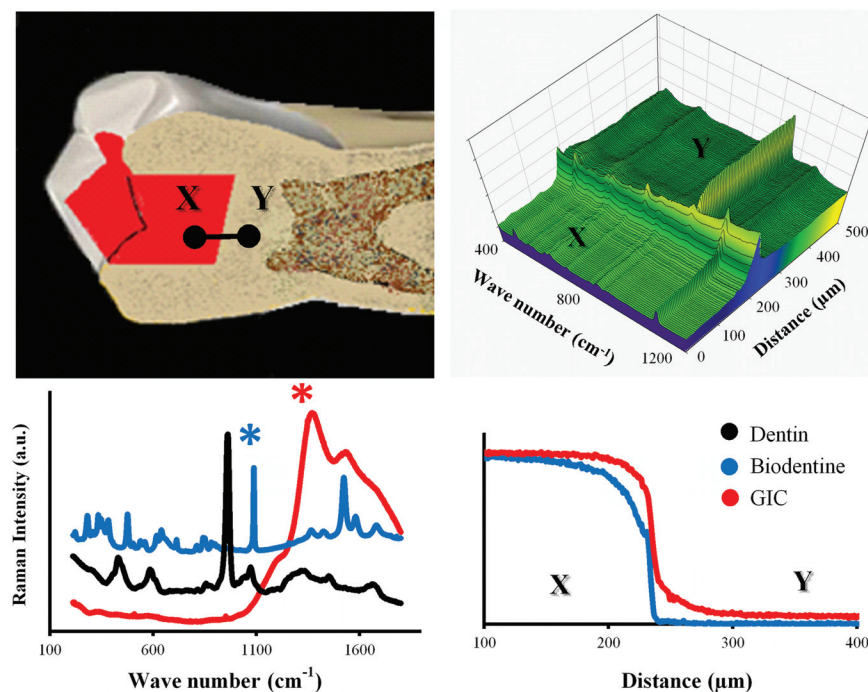


**Figure 4.** (upper left) Raman area maps were obtained for the dentin-cement interface in GIC and Biodentine filled teeth by StreamLine™ scanning in the direction from points X to Y. Raman spectral maps were analyzed with curve-fitting software which averaged each area map into a single line, where each point on that line was represented by an averaged Raman spectrum (upper right). From the cements' Raman spectra (lower left), representative characteristic peaks [ $1082\text{ cm}^{-1}$  and  $1262\text{ cm}^{-1}$  (marked with asterisks)] were designated for Biodentine and GIC cements, respectively. The average penetration depth was derived from the profiles of normalized Raman intensity of each peak, after they were generated from the curve-fitting software (lower right).

collagen component of interfacial dentin, explaining the concentration of fluorophores within this zone. This alkaline caustic effect or “caustic etching” has virtually no effect on the highly mineralized peritubular dentin, due to its lower collagen content, and is therefore represented by a dye-deficient area in the MIZ (Figs. 2a1, 2c1).

In the GIC samples, the richly dye-infiltrated layer formed beneath the interface was a result of the demineralizing effect of the PAA and tartaric acids on the inorganic dentin component. This inverse effect showed deeper infiltration of the cement-labeling fluorophore into the higher mineralized peritubular dentin (Figs. 2a2, 2c2), associated with lateral diffusion of the dye permeating from the pulp space through the demineralized peritubular dentin in that zone, leading to mixing of both dyes (Fig. 2c2). This mixing did not appear in the Biodentine samples (Fig. 2c1), where the dye permeating from the pulp failed to diffuse laterally in the MIZ, indicating an intact peritubular dentin.

Formation of an interfacial layer between the dentin and calcium silicate cements was previously reported (Sarkar *et al.*, 2005; Reyes-Carmona *et al.*, 2009; Han and Okiji, 2011). Those authors suggested that this layer forms within the dentin tubules and the interfacial region of the two substrates due to hydroxyapatite formation. Our findings also show that the mineral infiltration zone formed within the intertubular structure of the dentin, and that this layer is rich with carbonate ions. However, no direct comparison should be made, since the samples in our study were

kept in distilled water to delineate the effect of the cement alone, unlike the aforementioned studies, which used phosphate-buffered saline solutions.

Infiltration of calcium hydroxide/carbonate into interfacial dentin is associated additionally with mineral transfer, shown by the Raman maps (Fig. 4). The drop in Biodentine's Raman peak toward the pulp was gradual near the interface, corresponding to diffusion, but dropped suddenly at greater depth, suggesting the presence of a diffusion barrier: Calcium carbonate crystallization could be limiting further penetration. Dentin buffering may also explain this sudden drop. In GIC samples, the characteristic Raman peak dropped gradually throughout the whole penetration depth, which is consistent with diffusion products not being hindered by crystallization. This type of cements' diffusion into the intertubular dentin should be differentiated from “tubular diffusion” through the fluid-filled dentinal tubules, and therefore we suggest the term “intertubular diffusion” to describe it.

In summary, a richly dye-infiltrated layer appeared within the dentin under GIC and calcium silicate (Biodentine). However, its formation may be mediated by two opposite processes, one acidic and the other alkaline etching, respectively.

Raman spectroscopy confirmed the intertubular diffusion of carbonate from calcium silicate cement into dentin, leading to the formation of the “mineral infiltration zone” with mineral infiltration into the intertubular dentin, following the denaturing effect of the strongly alkaline cement. Comparison of the interfaces shows a dentin-mineral infiltration with the Biodentine, whereas polyacrylic and tartaric acids and their salts characterize GIC penetration. The use of stain-free SHG imaging technologies also indicates modification of the dentin collagen beneath tricalcium-silicate cement, all of which invalidates the null hypothesis regarding the relation of both materials with dentin.

## ACKNOWLEDGMENTS

This research was supported by Septodont. The authors acknowledge support from the Department of Health *via* the National Institute for Health Research (NIHR) comprehensive Biomedical Research Centre award to Guy's & St Thomas' NHS Foundation Trust with King's College London and King's College Hospital NHS Foundation Trust (Grant code, Guy's & St Thomas' NHS Foundation Trust & King's College London NIHR Biomedical Research Centre). This work was also supported by a Wellcome/ EPSRC Medical Engineering Centre grant. We thank Peter Pilecki and Dr. Salvatore Sauro for their valuable assistance. The author(s) declare no potential conflicts of interest with respect to the authorship and/or publication of this article.

## REFERENCES

- Andersen M, Lund A, Andreasen JO, Andreasen FM (1992). In vitro solubility of human pulp tissue in calcium hydroxide and sodium hypochlorite. *Dent Traumatol* 8:104-108.
- Andreasen JO, Farik B, Munksgaard EC (2002). Long-term calcium hydroxide as a root canal dressing may increase risk of root fracture. *Dent Traumatol* 18:134-137.
- Bowes JH (1950). The swelling of collagen in alkaline solutions; swelling in solutions of bivalent bases. *Biochem J* 46:530-532.
- Camilleri J, Montesin FE, Papaioannou S, McDonald F, Pitt Ford TR (2004). Biocompatibility of two commercial forms of mineral trioxide aggregate. *Int Endod J* 37:699-704.
- Camilleri J, Cutajar A, Mallia B (2011). Hydration characteristics of zirconium oxide replaced Portland cement for use as a root-end filling material. *Dent Mater* 27:845-854.
- Chen M, Chen W, Sun Y, Fwu P, Dong C (2007). Multiphoton autofluorescence and second-harmonic generation imaging of the tooth. *J Biomed Opt* 12:064018.
- Ferrari M, Davidson CL (1996). In vivo resin-dentin interdiffusion and tag formation with lateral branches of two adhesive systems. *J Prosthet Dent* 76:250-253.
- Han L, Okiji T (2011). Uptake of calcium and silicon released from calcium silicate-based endodontic materials into root canal dentin. *Int Endod J* 44:1081-1087.
- Ibáñez J, Artús L, Cuscó R, López Á, Menéndez E, Andrade MC (2007). Hydration and carbonation of monoclinic C2S and C3S studied by Raman spectroscopy. *J Raman Spectrosc* 38:61-67.
- Kemp GD, Tristram GR (1971). The preparation of an alkali-soluble collagen from demineralized bone. *Biochem J* 124:915-919.
- Kjellsen K, Justnes H (2004). Revisiting the microstructure of hydrated tricalcium silicate—a comparison to Portland cement. *Cement & Concrete Composites* 26:947-956.
- Lee SJ, Monsef M, Torabinejad M (1993). Sealing ability of a mineral trioxide aggregate for repair of lateral root perforations. *J Endod* 19:541-544.
- Martinez-Ramirez S, Frías M, Domingo C (2006). Micro-Raman spectroscopy in white Portland cement hydration: long-term study at room temperature. *J Raman Spectrosc* 37:555-561.
- No Authors Listed (2009). Biodentine Safety Data Sheet. Saint Maur des Fosses, France: Septodont. URL accessed on 3/2/2012 at: [http://www.sirawahelsinki.fi/uudet\\_septodont\\_pdf/Biodentine\\_safetydata.pdf](http://www.sirawahelsinki.fi/uudet_septodont_pdf/Biodentine_safetydata.pdf).
- Reyes-Carmona JF, Felipe MS, Felipe WT (2009). Biomineralization ability and interaction of mineral trioxide aggregate and white Portland cement with dentin in a phosphate-containing fluid. *J Endod* 35:731-736.
- Reyes-Carmona JF, Felipe MS, Felipe WT (2010). The biomineralization ability of mineral trioxide aggregate and Portland cement on dentin enhances the push-out strength. *J Endod* 36:286-291.
- Sarkar NK, Caicedo R, Ritwik P, Moiseyeva R, Kawashima I (2005). Physicochemical basis of the biologic properties of mineral trioxide aggregate. *J Endod* 31:97-100.
- Sun Y, Chen W, Lin S, Jee S, Chen Y, Lin L, *et al.* (2006). Investigating mechanisms of collagen thermal denaturation by high resolution second-harmonic generation imaging. *Biophys J* 91:2620-2625.
- Tay FR, Pashley DH, Rueggeberg FA, Loushine RJ, Weller RN (2007). Calcium phosphate phase transformation produced by the interaction of the Portland cement component of white mineral trioxide aggregate with a phosphate-containing fluid. *J Endod* 33:1347-1351.
- Taylor HW (1997). Cement chemistry. 2nd ed. London, UK: Thomas Telford Publishing.
- Torabinejad M, Hong CU, McDonald F, Pitt Ford TR (1995). Physical and chemical properties of a new root-end filling material. *J Endod* 21:349-353.
- Tsivilis S, Chaniotakis E, Kakali G, Batis G (2002). An analysis of the properties of Portland limestone cements and concrete. *Cement & Concrete Composites* 24:371-378.
- Watson TF (1999). Bonding glass-ionomer cements to tooth structure. In: *Advances in glass-ionomer cements*. Davidson CL, Mjör IA, editors. Germany: Quintessence Publishing Co., Inc.
- Watson TF, Cook RJ, Festy F, Pilecki P, Sauro SE (2008). Optical imaging techniques for dental biomaterials interfaces. In: *Dental biomaterials: imaging, testing and modelling*. Curtis RV, Watson TF, editors. Cambridge, UK: CRC Press.
- Weller RN, Tay KC, Garrett LV, Mai S, Primus CM, Gutmann JL, *et al.* (2008). Microscopic appearance and apical seal of root canals filled with gutta-percha and ProRoot Endo Sealer after immersion in a phosphate-containing fluid. *Int Endod J* 41:977-986.
- White JD, Lacefield WR, Chavers LS, Eleazer PD (2002). The effect of three commonly used endodontic materials on the strength and hardness of root dentin. *J Endod* 28:828-830.
- Wilson AD, Prosser HJ, Powis DM (1983). Mechanism of adhesion of poly-electrolyte cements to hydroxyapatite. *J Dent Res* 62:590-592.
- Young AM, Sherpa A, Pearson G, Schottlander B, Waters DN (2000). Use of Raman spectroscopy in characterisation of the acid-base reaction in glass-ionomer cements. *Biomaterials* 21:1971-1979.